Chinese Chemical Letters 32 (2021) 162–167

Contents lists available at ScienceDirect

Chinese Chemical Letters

journal homepage: www.elsevier.com/locate/cclet

Communication

ROS-responsive cyclodextrin nanoplatform for combined photodynamic therapy and chemotherapy of cancer

Die Jia[a,b,1], Xianbin Ma[a,b,1], Yi Lu[a,b], Xinyi Li[a,b], Shengxin Hou[a,b], Yuan Gao[a,b], Peng Xue[a,b], Yuejun Kang[a,b], Zhigang Xu[a,b,*]

[a] State Key Laboratory of Silkworm Genome Biology, School of Materials and Energy, Southwest University, Chongqing 400715, China
[b] Chongqing Engineering Research Center for Micro-Nano Biomedical Materials and Devices, Southwest University, Chongqing 400715, China

ARTICLE INFO

Article history:
Received 14 September 2020
Received in revised form 25 November 2020
Accepted 25 November 2020
Available online 1 December 2020

Keywords:
Chemotherapy
Photodynamic therapy
Synergistic therapy
Cyclodextrins
ROS-responsive

ABSTRACT

Cyclodextrin (CD) has special spatial structure and well biological safety, so it has been widely used for constructing CD-based nanoplatforms. Through functionalization, cyclodextrin can form various stimulus-response nanoplatforms, such as pH, temperature, redox, light and magnetic fields. In this study, we designed a highly sensitive reactive oxygen species (ROS)-responsive polymer PCP which encapsulated doxorubicin (DOX) and purpurin 18 (P18) to achieve the synergy of photodynamic and chemotherapy. The high content of reactive oxygen species (ROS) in the tumor microenvironment (TME) triggers the cleavage of the borate bond of MPEG-CD-PHB (PCP), thereby promoting the release of drugs. When irradiated with near-infrared laser, the photosensitizer P18 released by polymer micelles can produce reactive oxygen species to promote cell apoptosis. Compared with monotherapy, a series of experiments confirmed that our micelles had enhanced anti-cancer activity. This work was beneficial to the design of ROS-responsive materials and provides an effective strategy for the application of collaborative anti-tumor therapy.

In recent years, more and more researchers have paid attention to the use of nanoparticles as drug carriers to construct drug delivery systems [1,2]. Targeted therapy of nanomedicine was considered to be a promising strategy [3–5]. By constructing intelligent targeted drugs, therapeutic and imaging drugs can be specifically delivered to the tumor site. However, there were still some shortcomings in the treatment of tumors, such as poor drug targeting, low drug delivery efficiency and weak drug penetration in tissues [6–8]. Studies had found that the tumor microenvironment has the characteristics of low oxygen, low pH, high reactive oxygen species (ROS) levels and high expression of enzymes [9–12]. Using these characteristics of the tumor microenvironment as stimulating factors, designing a sensitive nano-drug system can improve the therapeutic effect of anti-tumor drugs [13–19].

Cyclodextrin (CD) had been widely used to construct drug delivery systems due to harmlessness and excellent biocompatibility [20,21]. Cyclodextrin had a special spatial structure, so it can form inclusion compounds with a variety of drugs, and further change the physical, chemical and biological properties of the drugs. For example, increased the solubility of hydrophobic drugs, improved the stability and bioavailability of the drugs, and reduced the toxicity and side effects of the drugs. At present, many stimulus-responsive nanomedicines have been designed using cyclodextrin, such as pH [22], temperature [23], redox [24–26] and enzymes, *etc.* [27,28]. But based on the characteristics of high reactive oxygen species (ROS) level, there were relatively few reports on cyclodextrin nanomedicine systems that respond to ROS [29]. Combined the cyclodextrin inclusion technology with the nano-drug delivery technology can not only utilize the unique inclusion principle of cyclodextrin, but also improve the solubility, stability and absorption of the drug, and reduce the stimulating effect of the drug. At the same time, nano prodrugs can further make drugs working synergistically to achieve sustained release, targeting and stability.

In this study, a ROS responsive CD-based micelles was proposed to deliver anti-tumor drugs (Fig. 1A). Mono(6-amino-6-deoxy)-β-cyclodextrin and hydrophilic polymPEG-NHS are first used for polymerization to generate MPEG-CD. Then MPEG-CD reacted with the compound PHB-CDI which contained borate bond to generate ROS responsive MPEG-CD-PHB (PCP) for wrap doxorubicin (DOX) and purpurin-18 (P18). Due to the high H_2O_2 concentration in the tumor microenvironment, when the drug

* Corresponding author at: State Key Laboratory of Silkworm Genome Biology, School of Materials and Energy, Southwest University, Chongqing 400715, China.
E-mail address: zgxu@swu.edu.cn (Z. Xu).
[1] These authors contributed equally to this work.

https://doi.org/10.1016/j.cclet.2020.11.052
1001-8417/

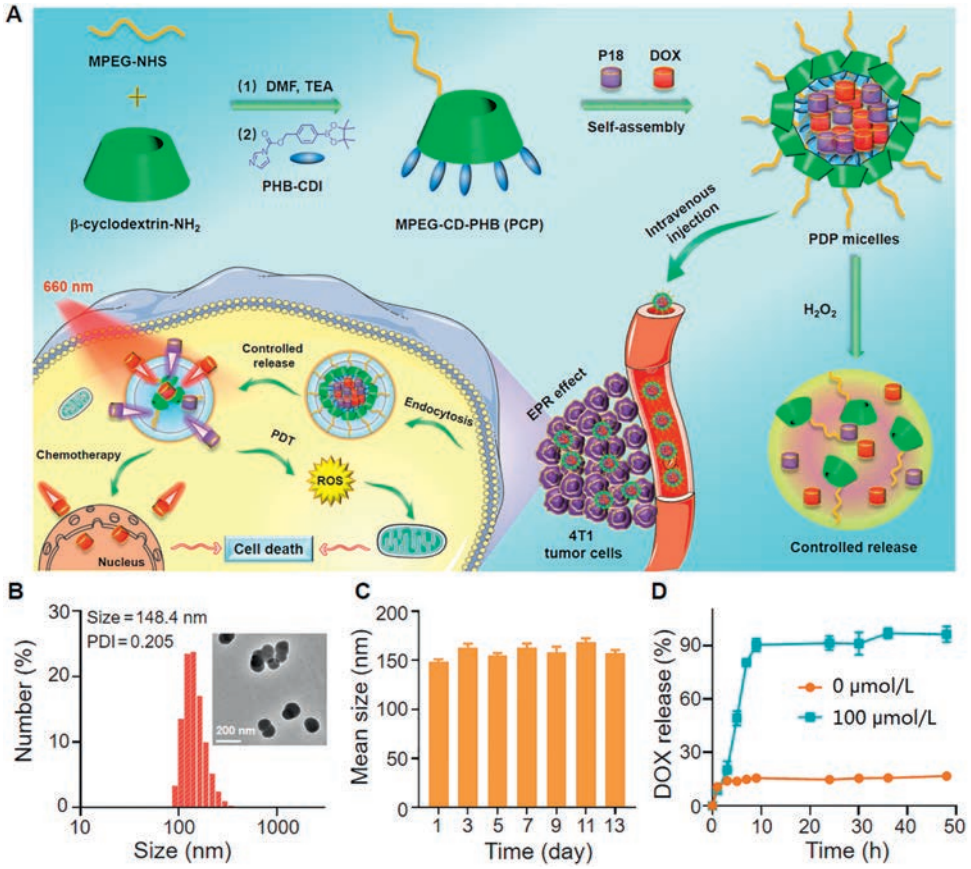

Fig. 1. (A) The synthesis route of β-CD-derived H_2O_2 responsive material (detailed chemical structure is shown in Supporting information), the self-assembly process of nanoparticles and their photo-activated combined treatment process. (B) TEM image and DLS size distribution histogram of PDP micelles. (C) Mean diameter distribution of PDP micelles under different incubation times. (D) H_2O_2 triggered DOX release of PDP micelles in PBS solution and 100 μmol/L of H_2O_2 solution. Data are presented as mean ± SD (n = 3).

entered the tumor microenvironment, DOX and P18 will be released from the PDP micelles. After the PDP micelles entered the tumor cell *via* enhanced permeability and retention (EPR) effect, the loaded DOX and P18 are released under the excitation of high concentration of ROS in tumor microenvironment (TME), which can produce cytotoxic ROS under NIR laser, thus achieved chemo-photodynamic therapy. Systematic experiments demonstrated that this PDP micells exhibited excellent anti-tumor efficacy and negligible systemic toxicity. Compared with other reported redox drug delivery systems [30,31], our nanocarrier had the following advantages: excellent stability, strong biocompatibility, stimulus-responsive release, fast phagocytosis, and effective tumor permeability, outstanding biological safety and excellent anti-cancer effect.

The micelles size and morphology of PCP micelles were measured by Transmission electron microscope (TEM) and dynamic light scattering (DLS), respectively. As shown in Fig. 1B, the average particle size of the PDP micelles was 148.4 nm. PDP micelles showed a nearly spherical morphology (TEM image), which might be due to the expansion of micelles in water. The corresponding zeta potentials of free DOX, free P18 and PDP were 13.2 ± 1.0, −11.5 ± 0.3 and −7.5 ± 7.5 mV, respectively (Fig. S5 in Supporting information). Then the hydrated particle size of the micelles was tested every two days, and there was no significant change in micelles particle size within 13 days (Fig. 1C). Under the effect of increasing permeability and retention rate (EPR), micelles had obvious advantages in extending the blood circulation time and increasing the permeability of drugs in tumor tissues [32,33]. The UV–vis spectrum was used to measure the encapsulation of drugs, and the UV–vis spectrum of PDP micelles showed all typical absorption peaks of DOX, P18 and PDP micelles (Fig. S6 in Supporting information). The fluorescence spectrum of PDP showed the characteristic emission peaks of DOX and P18, which meant that DOX and P18 had been successfully encapsulated (Fig. S7 in Supporting information). Similarly, the DLC of DOX and P18 were calculated to be 10.8% and 11.9%, respectively.

PCP was synthesized and characterized by the following steps. Firstly, as shown in Figs. S1-S4 (Supporting information), which show the ^{1}H NMR results of MPEG-CD, PHB-CDI and PCP, respectively. As shown in Fig. S2, ^{1}H NMR of PEG-CD in DMSO-d_6 showed the hydroxyl signal c (5.71 ppm), d (5.66 ppm) from β-CD and the methyl signal a (3.38 ppm) and methylene signal b (3.65 ppm) of MPEG-NHS, indicating the successful synthesis of MPEG-CD. Secondly, PHB reacts with *N,N*-carbonyldiimidazole (CDI) to form PHB-CDI, and the ^{1}H NMR result showed in Figs. S3 and S4 indicated that the final product PCP had been successfully synthesized.

Compared with normal cells, the high level of H_2O_2 in cancer cells can decompose the material and accelerate the release of drugs [34,35]. The in vitro drug release behavior of PDP micelles was tested by dialysis. The release rate of DOX from the PDP NP was measured by dialysis in different concentration of H_2O_2, which was used to simulate the reducing and oxidizing conditions in TME. As shown in Fig. 1D, when the concentration of H_2O_2 was 0 mmol/L, DOX is rarely released, which was related to the stability of PDP NP in physiological environment. However, when the H_2O_2 concentration increased to 100 μmol/L, more than 90% of the drug is released. This result showed that in the presence of H_2O_2, the

rupture of the borate bond in PDP micelles could accelerate the release of P18 and DOX.

The reactive oxygen species (ROS) produced by photosensitizer under laser irradiation can oxide the phospholipids on the cell membrane and DNA in the nucleus [36]. Singlet oxygen ($^1O_2$) is the main component of ROS, which can destroy targeted cancer cells in PDT [37]. DPBF can be rapidly oxidized to phthaloylbenzene under the presence of $^1O_2$. Therefore, the generation of singlet oxygen can be judged according to the change in absorbance of DPBF probe at 415 nm [38]. As shown in Fig. S8 (Supporting information), the absorbance of DPBF probe gradually decreased within 0–6 min, it indicated that the PDP micelles could generate $^1O_2$ under laser irradiation [39]. As the irradiation time increases, the absorbance gradually decreases, which indicated that PDP micelles can produce a large amount of $^1O_2$ to cause DPBF decomposition.

To further investigate the compatibility of PDP micelles, we conducted a blood hemolysis assay to determine the damage to red blood cells. As shown in Fig. S9 (Supporting information), the supernatants of the negative control group and the drug treatment group were transparent, the status of PDP micelles was almost consisted with the PBS group and the supernatants was transparent. When the concentration was 250 μg/mL, the hemolysis rate was still less than ~3%. These results indicate that the PDP micelle had good blood compatibility in blood circulation.

The cell uptake behavior was performed by confocal microscope. Using 4T1 cells, after incubating with PDP micelles (DOX concentration of 15 μg/mL) for 1 h and 4 h, the nucleus were stained with DAPI. It could be seen from Fig. 2A that the released DOX had entered the nucleus. The released P18 molecules remained in the cytoplasm. It showed that the cell uptake efficiency of PDP micelles was time-dependent. Fig. 2B showed that the DOX and P18 fluorescence intensity of PDP micelles gradually increased over time. At the same time, the cell uptake rate of PDP micelles was measured by flow cytometry (FCM). Initially, 4T1 cells were seeded in a 24-well culture dish at a density of 5×10^4 per well, and cultured overnight at 37 °C in 5% CO_2. The complete DMEM with 0.4 mL PDP micelles (DOX concentration is 8 μg/mL) were added, and were incubated at a constant temperature. 4T1 cells were cultured with PDP micelles for 1 h, 2 h and 4 h. After reaching the time point, the cells were washed with PBS, and then digested with trypsin, and DMEM terminated the digestion. PBS containing calcium and magnesium was added and collected for FCM analysis, the cell uptake rate of PDP micelles reached 96.87% after 4 h. (Fig. 2C). It could be seen that the phagocytosis rate increased with the increase of culture time. It showed that micelles could be swallowed quickly.

In order to study the anti-cancer properties of PDP micelles, we used 4T1 cells to evaluate *in vitro* cytotoxicity. Free DOX, Free P18 and PDP micelles were added to 4T1 cells respectively. The groups (Free P18 and PDP micelles) were treated with laser irradiation after incubated with 4T1 cells for 4 h, and the cells without treatment were set as controls. All experimental groups showed a concentration-dependent ability to induce cancer cell death and PDP with laser group showed more toxic than other groups. For example, different pharmaceutical formulations containing 5 μg/mL DOX, 8.7 μg/mL P18, free DOX, PDP, P18 + laser, PDP + laser interacted with 4T1 cells for 4 h, and then were irradiated with 660 nm (0.5 W/cm^2) laser for 5 min. The cell survival rates of free DOX, PDP, P18 + laser, and PDP + laser were about 40.89%, 33.74%, 61.28% and 17.17%, respectively. It could be seen from the

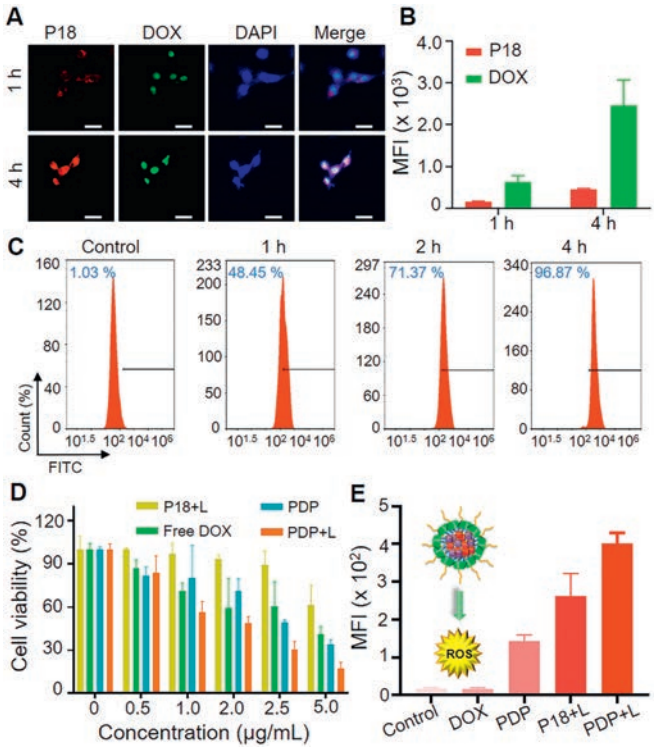

Fig. 2. Cellular uptake, cytotoxicity and ROS generation of PDP micelles *in vitro*. (A) Confocal images and (B) average fluorescence intensity of 4T1 cells incubated with PDP micelles for 1 h and 4 h. Scale bar: 50 μm. (C) Flow cytometry analysis of the cellular uptake of DOX-loaded PDP micelles for 1 h, 2 h and 4 h, respectively. (D) Cell viabilities of 4T1 cells treated with different concentrations of Free P18 + laser (P18+L), PDP + laser (PDP+L), PDP, and Free DOX for 24 h under 660 nm laser irradiation (0.5 W/cm, 5 min). (E) Quantification of ROS produced in cells. Data are presented as mean ± SD ($n = 3$).

experimental results that when the drug concentration was low, the tumor cell survival rate was 17.17%, indicating that the combination of PDT and chemotherapy had significant tumor ablation effect (Fig. 2D).

Because of its highly selective $^1O_2$, the singlet oxygen (SOSG) fluorescent probe was applied to assess ROS level in cells. In the presence of singlet oxygen, the probe could emit green fluorescence similar to fluorescein. As shown in Fig. 2E and Fig. S10 (Supporting information), after 4 h of incubation with DOX, P18 and PDP drugs, P18 and PDP were given a certain amount of light (660 nm, 0.5 W/cm^2, 5 min). It could be seen that the PDP plus laser treatment group green fluorescence was the strongest, while green fluorescence in other controls was much weaker.

The cellular internalization pathways of PDP micelles were also conducted by staining lysosome and mitochondria. As shown in Figs. S11 and S12 (Supporting information), lysosomes were stained with Lyso-Tracker Blue, and mitochondria were stained with Mito-Tracker Orange. After 1 h and 4 h of drug incubation, the fluorescence intensity of DOX and P18 increased slightly with the increase of time, indicateing that the time-dependent process of PDP micelles entering the cells, which was consisted with our above FCM results. Fig. S11B showed the average fluorescence intensity of DOX and P18 at different times in the mitochondrial colocalization experiment. Fig. S12B showed the average fluorescence intensity of DOX and P18 at different times in the lysosomal colocalization experiment.

The efficiency of anti-cancer micelles were affected by complex tumor microenvironment in solid tumor. To further study this feature, we established a multicellular sphere of 4T1 cells to study the ability of micelles to penetrate solid tumor tissue. As shown in Fig. 3A, after incubateing with 4T1 multicellular spheres for 6 h, the red fluorescence of P18 and green fluorescence of DOX could be detected at different depths by scanning confocal images. Fig. 3B showed the average fluorescence values of DOX and P18 at different depths of tumor spheres, which indicated that multi-drug micelles had good permeability to solid tumors. Fig. 3C showed the fluorescence signal intensity distribution of DOX and P18 channels at a depth of 40 μm.

The distribution of PDP micelles were measured by fluorescence imaging on the 4T1 tumor-bearing mice [40]. PDP and free P18 were injected through the tail vein of mice at the same dose of P18, and whole-body fluorescence imaging was performed 24 h later, as shown in Fig. 3D. It could be seen from the imaging diagram that 24 h after the injection of the drug, the mice in the PDP group presented obvious fluorescence, indicating that PDP micelles could be enriched in the tumor lesion. Fig. 3E and Fig. S13 (Supporting information) showed the quantification of the separated tumor and major organs (heart, liver, spleen, lung and kidney). It could be seen from this figure that PDP micelles could effectively accumulate than free P18 through prolong blood circulation at the tumor site.

In addition, the *in vivo* biocompatibility test of free P18, free DOX and PDP micelles was carried out on healthy Kunming mice. Typical blood indicators including WBC, LYM, RBC, RDW, HCT, MCHC, HGB, MPV and PLT were tested. The control groups were injected with normal saline and the biochemical parameters of the mice were tested after 7 days of treatment with PDP micelles. Compared with the PBS group, the parameters of the PDP

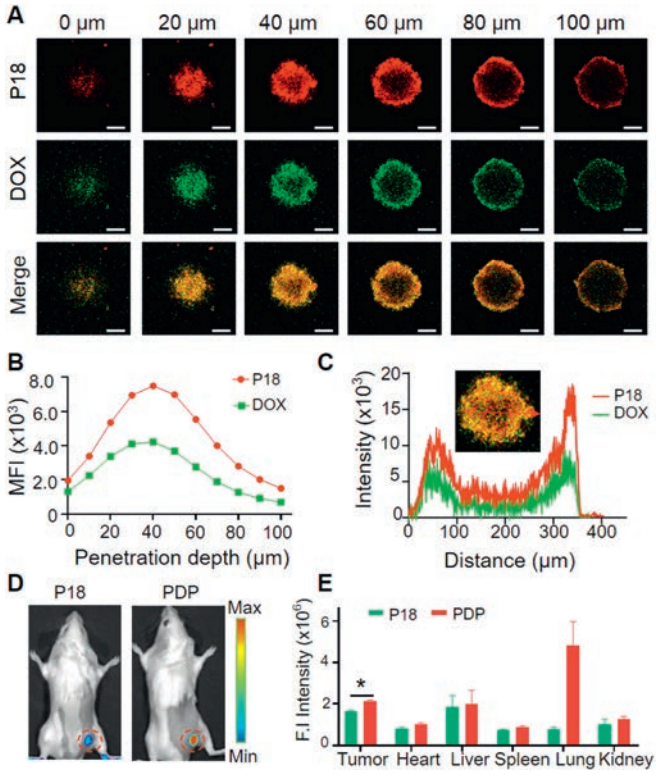

Fig. 3. (A) Confocal microscopy imaging of PDP micelles penetrating the 4T1 tumor spheres for 6 h. Scale bar: 100 μm. (B) The average fluorescence value of DOX and P18 at different depths in the tumor sphere. (C) Corresponding to the fluorescence signal intensity distribution of the DOX and P18 channels of the tumor sphere when the depth is 40 μm. (D) *Ex vivo* fluorescence imaging of PDP micelles distribution in tumor, 4T1 tumor-bearing BALB/c mice after injection with free P18, PDP micelles (P18 concentration: 5 mg/kg) *via* tail veins. (E) Quantitative comparison of P18 signal intensity in different organs. Data are presented as mean ± SD (n = 3).

treatment group were kept within a reasonable range (Fig. S14 in Supporting information). It showed that the designed micelles had good blood compatibility and had no obvious negative effects on the blood chemistry of mice. Simultaneously, the body weights of the mice were recorded every day (Fig. S15 in Supporting information). The weight of the mice did not fluctuate significantly, indicating that the drug had good biological safety.

Benefiting from excellent cytotoxicity *in vitro* and effective accumulation of PDP micelles in tumor site, we further investigated the anti-tumor activity on 4T1 tumor-bearing mice. The schematic diagram of anti-tumor experiments was shown in Fig. 4A. Typically, when the tumor volume reached approximately 100 mm^3, all of the mice were randomly divided into five groups: (1) saline, (2) free DOX, (3) free P18 + laser, (4) PDP, (5) PDP + laser. The tumor volumes were recoded every day. The drug was injected every three days for a total of three injections, and the tumors were removed from the mice sacrificed on the 14^{th} day for further analysis. As shown in Fig. 4B, it could be observed that the mouse tumor volume in the saline group grew rapidly compared with other groups. On the contrary, the PDP micelle group showed significant tumor suppressor effect. A similar trend of results was observed in the tumor weight in Fig. 4C. Fig. S16 (Supporting information) showed the change in body weight during the treatment, and the body weight of mice showed no significantly fluctuate. In addition, as shown in Fig. 4D, hematoxylin and eosin (H&E) and TdT-mediated dUTP nick-end labeling (TUNEL) stained tumor tissue photos also verified the experimental results. Fig. S17 (Supporting information). Figs. 4E and F showed the quantification of TUNEL and Ki67 images using Image J. It could be observed that the PDP-treated tumors showed higher apoptosis. After treatment, no obvious pathological abnormality was found in the H&E sites of the heart, liver, spleen, lung and kidney (Fig. S18 in Supporting information). All about these results proved that the prepared PDP micelles had excellent biosafety *in vivo*.

In short, we proposed a ROS-responsive biodegradable nanomaterial PCP, which had the advantages of stimulating response, synergistic treatment, low toxicity and good biocompatibility. By encapsulating the photosensitizer P18 and the chemotherapeutic drug DOX in the H_2O_2-responsive material PCP, a successful anti-tumor therapy was obtained. Cell uptake and MTT experiments were used to study the anti-cancer efficacy *in vitro*. Based on these results, this work helped to provide effective strategies for the application of synergistic anti-tumor therapy.

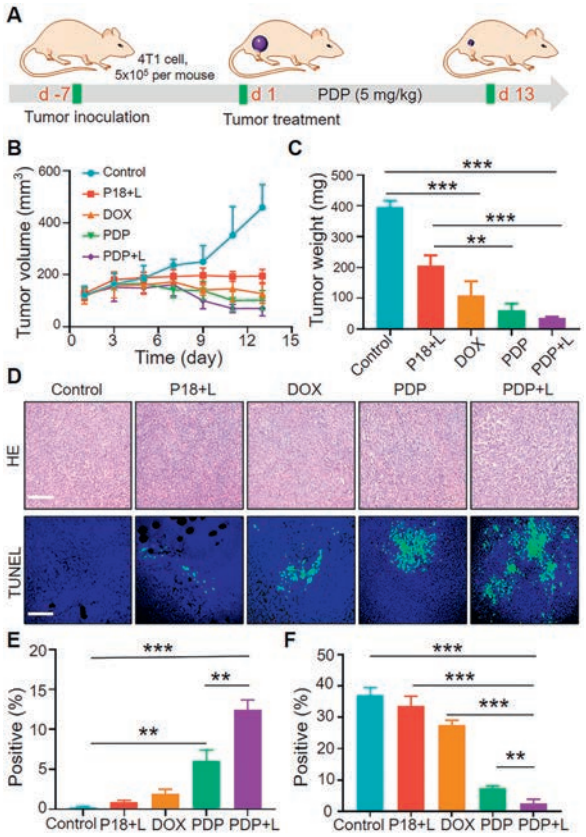

Fig. 4. In the 4T1 tumor model, the *in vivo* anti-tumor performance of chemotherapy and photodynamic therapy (660 nm, 0.5 W/cm^2, 5 min). (A) Timetable for *in vivo* anti-tumor efficacy trials. (B) Tumor volume change curve for different treatments. (C) The tumor weight after different treatments. Data are presented as mean ± SD (n = 5). (D) H&E and TUNEL slices of tumor staining image. Scale bars: 200 μm. (E) Quantification of tumor TUNEL and (F) Ki67 used image J. Free. P18+L: P18 + laser, PDP+L: PDP + laser. Data are presented as mean ± SD (n = 3).

Declaration of competing interest

The authors declare that they have no known competing financial interests or personal relationships that could have appeared to influence the work reported in this paper.

Acknowledgments

This work was financially supported by the National Natural Science Foundation of China (Nos. 51703187, 31671037) and the Basic and Frontier Research Project of Chongqing (No. cstc2018jcyjAX0104).

Appendix A. Supplementary data

Supplementary material related to this article can be found, in the online version, at doi:https://doi.org/10.1016/j.cclet.2020.11.052.

References

[1] A.N. Zelikin, C. Ehrhardt, A.M. Healy, Nat. Chem. 8 (2016) 997–1007.
[2] G. Yu, X. Chen, Theranostics 9 (2019) 3041–3074.
[3] L. Yu, Y. Chen, H.R. Chen, Chin. Chem. Lett. 28 (2017) 1841–1850.
[4] Z. Xu, X. Ma, Y.E. Gao, et al., Mater. Chem. Front. 1 (2017) 1257–1272.
[5] T. Miao, J. Wang, Y. Zeng, et al., Adv. Sci. 5 (2018) 1700513.
[6] J. Du, H. Li, J. Wang, Acc. Chem. Res. 51 (2018) 2848–2856.
[7] Y. Zhao, J. Peng, J. Li, L. Huang, et al., Nano Lett. 17 (2017) 4096–4100.
[8] D. Chen, Z. Zhong, Q. Ma, et al., ACS Appl. Mater. Interfaces 12 (2020) 26914–26915.
[9] J. Liu, Y. Huang, A. Kumar, et al., Biotechnol. Adv. 32 (2014) 693–710.
[10] L.F. Han, L.J. Hu, F.L. Liu, Asian J. Pharm. Sci. 14 (2019) 531–542.
[11] M. Upreti, A. Jyoti, P. Sethi, Mol. Cancer Res. 2 (2013) 309–319.
[12] E.S. Nakasone, H.A. Askautrud, T. Kees, et al., Cancer Cell 21 (2012) 488–503.
[13] P. Liang, X. Huang, Y. Wang, et al., ACS Nano 12 (2018) 11446–11457.
[14] K.L. Ding, C.X. Zheng, L.L. Sun, et al., Chin. Chem. Lett. 31 (2020) 1168–1172.
[15] M. Kanamala, W.R. Wilson, M. Yang, Biomaterials 85 (2016) 152–167.
[16] Q. Hu, W. Sun, Y. Lu, et al., Nano Lett. 16 (2016) 1118–1126.
[17] S. Bai, L.L. Yang, Y.J. Wang, et al., Small 16 (2020) 2000214.
[18] X.X. Shi, Y. Zhang, Y. Tian, et al., Small Methods (2020) 2000416.
[19] S.T. Gao, G.S. Tang, D.W. Hua, J. Mater. Chem. B 7 (2019) 709–729.
[20] E.K. Lim, T. Kim, S. Paik, et al., Chem. Rev. 115 (2015) 327–394.
[21] W. Fan, B. Yung, P. Huang, et al., Chem. Rev. 117 (2017) 13566–13638.
[22] D. Chen, Q. Yu, X. Huang, et al., Small 16 (2020) 2001059.
[23] X. Song, Y. Wen, J.L. Zhu, et al., Biomacromolecules 17 (2016) 3957–3963.
[24] L. Lin, H. Gong, R. Li, Adv. Sci. 7 (2020) 1903138.
[25] L. Wei, Y. Zhao, X. Hu, et al., ACS Cent. Sci. 6 (2020) 404–412.
[26] B. Hou, L. Zhou, H. Wang, et al., Adv. Mater. 32 (2020) 1907210.
[27] J. Lee, E.T. Oh, H. Yoon, et al., Nanoscale 9 (2017) 6901–6909.
[28] Y. Yang, Y.M. Zhang, Y. Chen, et al., Sci. Rep. 6 (2016) 19212.
[29] Q. Zhang, F. Zhang, Y. Chen, et al., Chem. Mater. 29 (2017) 8221–8238.
[30] T. Zhang, J. Yao, J. Tian, et al., Chin. Chem. Lett. 31 (2020) 1129–1132.
[31] F. Bahrami, M.J. Abdekhodaie, F. Behroozi, et al., Chin. Chem. Lett. 57 (2020) 101510.
[32] P.F. Zhang, J.Q. Wang, H. Chen, et al., J. Am. Chem. Soc. 140 (2018) 14980–14989.
[33] S.J. Leung, M. Romanowski, Adv. Mater. 24 (2012) 6380–6383.
[34] M. Wang, S. Sun, C.I. Neufeld, Angew. Chem. 126 (2014) 13662–13666.

[35] Z.Y. Cao, Y.C. Ma, C.Y. Sun, Chem. Mater. 30 (2018) 517–525.
[36] Y.N. Antonenko, A.V. Avetisyan, L.E. Bakeeva, et al., Biochemistry 73 (2008) 1273–1287.
[37] M. Dong, X. Xiao, Z. Su, et al., Small 15 (2019) 1900212.
[38] Y. Cheng, A.C. Samia, J.D. Meyers, J. Am. Chem. Soc. 130 (2008) 10643–10647.
[39] X. Liu, J. Xiang, D. Zhu, et al., Adv. Mater. 28 (2016) 1743–1752.
[40] Q. Wei, Y. Chen, X. Ma, et al., Adv. Funct. Mater. 28 (2018) 1704634.